Fatigue life analysis of wheel-rail contacts at railway turnouts using finite element modelling approach.

To cite this article: Y D Jelila *et al* 2021 *IOP Conf. Ser.: Mater. Sci. Eng.* **1201** 012047

Fatigue life analysis of wheel-rail contacts at railway turnouts using finite element modelling approach.

Y D Jelila[1, *, 3], H G Lemu[2, *], W Pamuła[1] and G G. Sirata[3, 4]

[1] Faculty of Transport and Aviation Engineering, Silesian University of Technology, Poland.
[2] Faculty of Science and Technology, University of Stavanger, Norway.
[3] Faculty of Mechanical Engineering, Jimma University, Ethiopia.
[4] Faculty of Materials Engineering, Silesian University of Technology, Poland.

Corresponding authors email: [1, *] yohanis.jelila@ju.edu.et and [2, *] hirpa.g.lemu@uis.no

Abstract. The article deals with wheel-rail contact analysis at railway turnout using a finite element modelling approach. The focus is understanding the wheel-rail contact problems and finding the means of reducing these problems at railway turnouts. The main aim of the work reported in this article is to analyse fatigue life and simulate the wheel-rail contact problems for a repeated wheel loading cycle by considering the effect of normal and tangential contact force impact under different vehicle loading conditions. The study investigates the impact of tangential contact force generated due to different-angled shapes of the turnout and aims to reveal how it affects the life of contacting surfaces. The obtained results show that the maximum von-Mises equivalent alternating stress, maximal fatigue sensitivity, and maximum hysteresis loop stresses were observed under tangential contact force. These maximum stresses and hysteresis loops are responsible for rolling contact fatigue damage, and excessive deformation of the wheel-rail contact surface. At a constant rotational velocity, the tangential contact force has a significant impact on the fatigue life cycle and wheel-rail material subjected to fatigue damage at lower cycles compared to the normal contact force. The finite element modelling analysis result indicated that the contact damages and structural integrity of the wheel-rail contact surface are highly dependent on contact force type and can be affected by the track geometry parameters.

Keywords: Finite element modelling, wheel-rail contact, contact force, stress and strain life-based fatigue, railway turnout.

1. Introduction

Railway turnouts (switches & crossings) are integral parts of a railway network which offer the capability to control the traffic flows through connection of various tracks. However, due to the maintenance and replacement of switch tracks and crossings, this control capability is very expensive.

The crossing rails profiles can vary along the crossing panels to make it possible for the vehicle to change between tracks. The wheel passage on different rail profiles interacts variously, which is expressed using contact forces, boundary conditions of the wheel/rail contact. The combination of crossing rails to support wheel loads together increase the frequency of multiple contact in railway crossings when wheels move from a frog rail to a wing track in a crossing panel, normal contact conditions are disturbed.

Dynamic interactions between wheel and rails at the crossing turnouts, which include a high impact load caused by the dip angle in the vertical trajectory of the wheel, lead to material deterioration of the

passageways in both the face-up and trailing directions [1, 2]. The design of crossings includes an inherent geometric discontinuity that causes unexpected vibration and high impact forces on the wheel-rail. Subsequently, crossings are critical components that are likely to exacerbate both wheel and rail degradation [3].

The conventional turnout structure with a fixed crossing has a modified rail profile to accommodate the change in the geometry of the wheel-rail contact. This makes turnout a vulnerable part of the railway structure and an important factor limiting the life of wheel/rails. Being one of the weakest points in the railway system, turnout absorbs a high percentage of the budget for the maintenance and repair [4].

To improve and optimize, the dynamic interaction between wheel-rail in the turnout transition zone, effectively and ensure that the turnout offers a safe, long-lasting service throughout its life cycle, several studies were conducted over last four decades. For instance, Sysyn et al. [5] conducted experimental investigation of deterioration mechanisms, rail contact fatigue damage based on inertial and geometric measurements of one crossing during its full lifecycle. The machine learning technique t-distributed stochastic neighbour embedding was also applied in this case to find a small cluster of highly influential loadings that indicate the location of the future damage zone. Chen et al. [6] investigated the impact of wheel profile evolution on wheel-rail dynamic interaction and surface-induced rolling contact fatigue in turnouts by developing a model of the vehicle-turnout coupling and analysed the wheel-rail dynamic interaction in turnouts.

In the study reported in [7], three methodologies are used to evaluate the performance of railway crossing rails after prolonged service. The methods are 3D profile and hardness measurements, finite element simulation of wheel/rail interaction, and numerical prediction of rail degradation. The authors discovered that the crossing underwent a run-in process in the direction of the primary traffic flow, which manifested as a widening of the running band, an enlargement of the contact patch size, a decrease in contact stress, and eventually a decrease in plastic deformation and wear. However, the minor traffic heading contributed to increased plastic deformation and wear on the wheel/rail assembly which is very contradictory concept.

Numerical prediction of accumulated plastic deformation and wear in railway crossings has been developed [8]. During each wheel transition between the wing rail and the crossing nose, high magnitudes of contact pressure and slip are generated in the wheel–rail contacts, causing damage. Wei et al. [3] elaborated a method for evaluating the performance of railway crossing rails after long-term service. The authors conclude that the widening of the running band, which occurs when the contact patch is subjected to large stresses is positively correlated with the contact stress size and plastic deformation in the traffic direction. The residual stress in the rail material, axle load statistics, train speed, and moving direction were not investigated in detail as contributing factors to wheel/rail interaction problems.

Xu and Liu [9] study, the vehicle-track interaction at the railway crossing using a matrix coupled model. To enhance both the efficiency and the accuracy of the simulation, the authors designed a two-point contact model of the transition of the wheel load in the crossing panel. They also examine the impact of track irregularities on vehicle-track interaction and find that irregularities in the track primarily impact wheel–rail interaction, whereas rail geometry variance takes the lead in influencing wheel-crossing interaction. However, in this work, the impact of interacting force due to track irregularities and geometry discontinuity is not investigated.

A detailed investigation into the causes of a recent railway turnout failure and their possible links to ongoing and future research on the Great Britain network has been conducted from 2011 to 2017 [10]. The author provided information on the causes for failure and research needs for the next generation of switches and crossings.

The literature review shows that most of the studies are focused on the analysis of the strain dynamics of railway crossing, railway crossing steel grade analysis, numerical prediction and multi-body dynamics simulations of wheel-rails contact. The impact of wheel loading during the transition of turnout, the impact of geometry discontinuity on the contact pressure distribution and the force generated

due to transition geometry, which has a great impact on the dynamics and life of wheel-rail contact have not been investigated in detail.

In this paper, the impact of contact force generated i.e., normal and tangential contact force due to railway turnouts crossing geometry, on the fatigue life, contact pressure/stress, cyclic stress, and fatigue sensitivity of wheel/rails, is investigated using the finite element method (FEM) approach.

2. Materials and methods

The impact of contact force on the properties of wheel-rail interaction is modelled using FEM software. A 3D geometric model of wheel-rail contact at turnouts of the railway is proposed. The model framework is based on the specifications of Addis Ababa light railway transit (AALRT) [11]. The proposed design of the 3D model is imported to ANSYS workbench for contact condition analysis and simulation.

Wheel-rail contact modelling at rails turnouts based on the wheelset, track, rail specification of the vehicle dimension as it moves along curved track is investigated. For the contact analysis, S1002 wheel and international union of railways (UIC) 60 rail profiles that are frequently used are examined by finite element analysis (FEA). The model of the wheel has a nominal rolling radius of 330 mm [12]. The crossing nose is mounted at the centre of track and located at an angle of 53.5 degrees downward from the horizontal direction to divert the direction of motion of track. The finite element modelling of wheel-rail contact analysis is performed using the static structural analysis toolbox of the ANSYS workbench. A finite element model for wheel-rail rolling contact is developed on the most critical section of railway track i.e., on railway turnouts to calculate elastic-plastic FEA results such as fatigue life (sensitivity life, damage), alternating contact stress and hysteresis response in the wheel-rail contact regions under normal and tangential contact force.

ANSYS inbuilt wheel-rail material properties of steel alloys are used for wheel-rail contact analysis to determine the resistance to fatigue loading and to what degree wheel-rails provide intended operation. The wheel-rail mechanical properties of steel alloys and geometrical properties are tabulated, as shown in Table 1, based on the Ethiopian railway specification [13]. On this basis, the plastic, bilinear kinematic hardening material properties from the engineering data sources of the ANSYS workbench are selected to represent the repeated loading condition and interpolate the properties between stress-number of cycles, S-N curve of the selected wheel-rail material.

Table 1. Wheel-rail materials property and geometrical parameter of Addis Ababa light rail transit.

Material property	Corresponding value	Geometric Parameter	Specification
Density	7820 kg/m^3	Rail inclination at bottom	1/40
Poison's ration	0.3	Lateral displacement	7.5 mm
Tensile/compressive strength	540 MPa	Max. super elevation	120 mm
Ultimate tensile strength	880 MPa	Min. horizontal radius of curve	50 m
Yield strength	500 MPa	Max. vertical radius of curve	1000 m
Young modulus	210 GPa	Track gauge	1435 mm
Shear modulus	80 GPa	Rail type	50 kg
Tangent modulus	400 MPa	Wheel diameter(new)	660 mm
		Wheelbase	1900 mm

Throughout this article, the following assumptions are made on which the fundamental analysis of the FE depends.

- The contact between the surface is not perfectly smooth and the coefficient of friction of 0.2 is assumed.
- The normal and tangential problems are threated independently, though it is not practical to consider tangential force without normal force. Therefore, normal contact forces are assumed to be constant.

- The minimum horizontal radius of the curvature of rail tracks is 50 m and reduction scale factor of 1/20 is assumed for geometric modelling and better windows workspace visualization.
- Constant rotational speed of train wheel of 70km/hr or 562rpm is assumed for tangential force analysis.

2.1. Finite element analysis set up

In this setup, four boundary conditions (contact region formulations, meshing, fixed support and loading conditions) are examined and applied in the design module at the necessary locations accordingly. A contact region settled between wheel and rail, is defined by creating connections using the contact tool in design module. The contact tool connection with frictional contact surface is defined and friction coefficient of 0.2 is assumed. As illustrated in Figure 1(a), four contact regions are examined for the wheel (target body, blue colour surface) and rail (contacting body, red colour surface) interaction along the straight and curved track on the front and rear wheelset of the vehicle. The geometry is meshed using triangular type elements, (see Figure 1(b)) with the maximum resolution of 7 and the mesh refinement at wheel-rail interface section with a maximum refinement of 3 and element size of 5mm. The refinement resolution and element size of 5 mm are assumed to be enough for FE analysis interpretations.

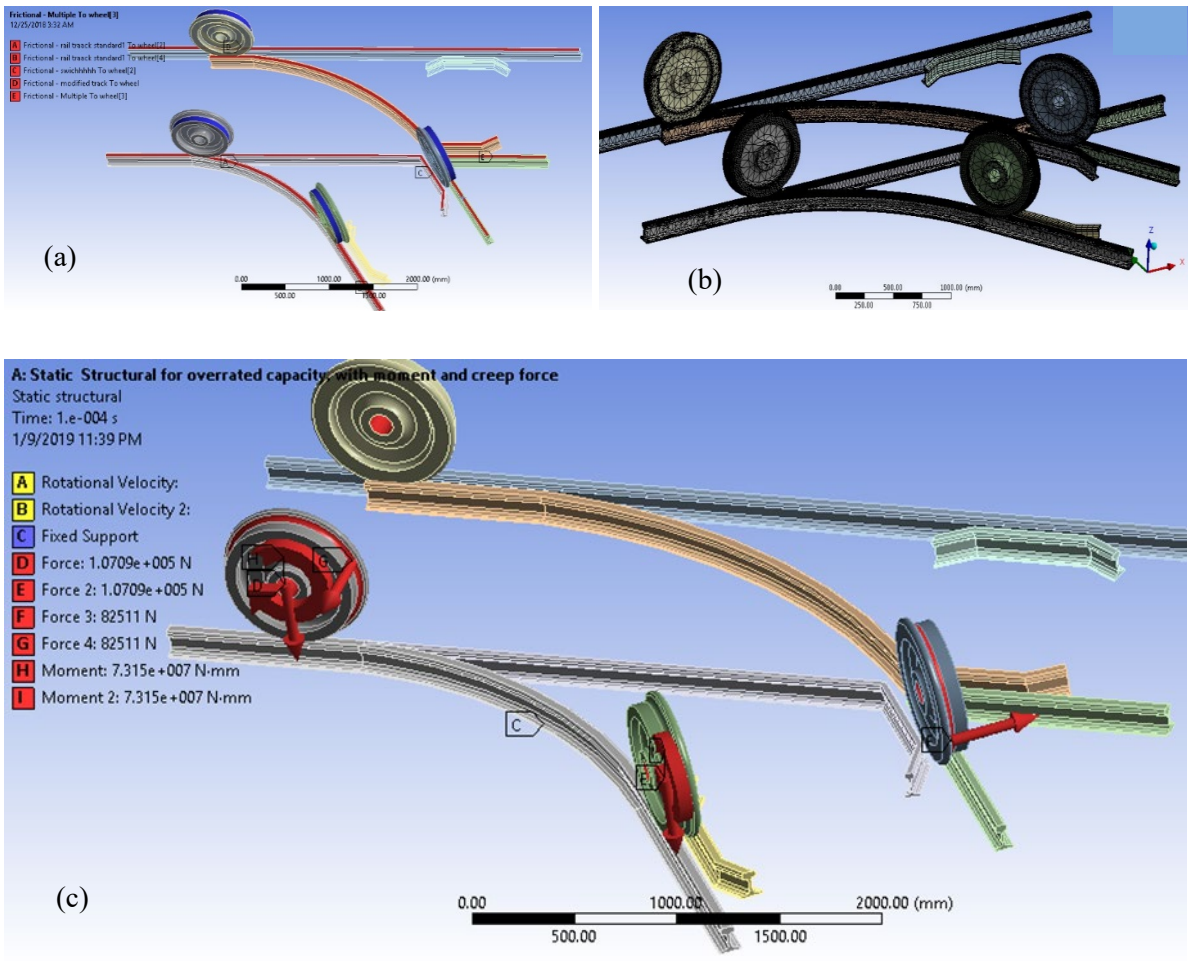

Figure 1. (a) Wheel-rail contact region formulation, (b) meshed geometry at railway turnout and (c) loading boundary conditions.

The fixed support boundary condition is applied because of loading boundary conditions. In a practical case, the railway is fixed to sleepers using various fittings like keys and spikes to maintain its

static equilibrium. To represent this property in ANSYS Workbench, the rail model surfaces are fixed to the ground.

The loading boundary condition includes normal and tangential contact forces. The normal contact force on wheel is assumed to be constant when the wheel rolls either on the straight or curved track. The normal contact forces are a point contact Hertzian problem caused by the vehicle's weight and are applied perpendicular to the rail top surface. The normal contact forces are calculated based on this concept. Tangential contact force is formed and transmitted due to torque applied, surface friction in contact, and when the wheel deviates from pure rolling during traction, braking, or curving in the contact patches. During this time, the velocity difference between the wheel and rail elements causes the relative slip of contact. The tangential contact forces are not constant when the wheel rolls over curved track, they are highly affected by geometry of wheel and curved track. As it is indicated in Figure 1 (c), when the vehicle enters turnout x-section, tangential contact force keeps the wheel on the track using it wheel flange design geometry and these forces are opposite in the x-section. Tangential contact forces are calculated based on Kalker's linear theory of contact [14]. The normal contact force of 91.54 kN, 104.00 kN, 107.09 kN, and the tangential contact force of 70.53 kN, 80.13 kN, 82.51 kN were used in this investigation for AALRT under empty, optimal, and overrated vehicle loading situations, respectively. The rotation effect of each train wheel is examined with constant spin moment and rotational velocity of 73.15 kNm and 562.40 rpm respectively.

2.2. Setting up for a solution

Setting up a solution is the last stage in solving the wheel-rail contact analysis using FEM. At this step, the type of contact analysis such as stress life-base and strain life-base with their mean correction factor are set based on type analysis targeted.

Stress-life fatigue analysis is based on S-N (stress-number of cycle) curves and thus addresses High Cycle Fatigue (HCF), which is defined as greater than 10^5 cycles life as indicated in equation (1) [15]. To consider various stress correction factors, such as the mean stress correction factor, and to relate them to experimental data, the Gerber theory is an excellent choice for ductile materials, and thus, selected for this analysis. The Gerber theory assumes that both negative and positive mean stresses are the same [16], it is employed in the ANSYS fatigue module. Gerber empirical formula is indicated in equation (2) and graphical interpretation of mean stress correction factor is plotted in Figure 2(a).

$$\frac{\Delta\sigma}{2} = \sigma_f{}'(2N_f)^b \tag{1}$$

Where $\Delta\sigma/2$ is stress amplitude, $2N_f$ is reversals to failure (1 rev = ½ cycle), σ_f' is fatigue strength coefficient, b is fatigue strength exponent (Basquin's exponent). Parameters σ_f' and b are fatigue properties of the material.

$$\frac{\sigma_{alt}}{S_e} + \left[\frac{\sigma_m}{S_u}\right]^2 = 1 \tag{2}$$

Where σ_{alt} is alternating stress, S_e is endurance limit strength, S_u is ultimate strength and σ_m, is the mean stress.

Strain-life-based fatigue is based on the strain-life relationship equation and addresses LCF (Low Cycle Fatigue), but also works with a higher cycle count. Low cycle fatigue is a term that is frequently used [17, 18]. Strain-life parameters are values for a particular material that best fit the equation to the measured data. Manson-Coffin determined a link between the strain-life defined by material properties and its fundamental relationship [19]. The strain-life relationship shown in equations (3a and 3b) is used to map the strain curve. In this study, the Morrow model is used to analyse more elastic and less plastic behaviour of the wheel-rail material.

Morrow's mean stress correction model predicts low plastic strain values, where elastic strain dominates [20]. The correction also reflects the trend that mean stresses have little effect on shorter lives, where plastic strains are large, as shown in equation (3b) [21].

$$\frac{\Delta\varepsilon}{2} = \frac{\sigma_f'}{E}(2N_f)^b + \varepsilon_f'(2N_f)^c \quad (3a)$$

$$\frac{\Delta\varepsilon}{2} = \frac{\sigma_f' - \sigma_m}{E}(2N_f)^b + \varepsilon_f'(2N_f)^c \quad (3b)$$

Where $\frac{\Delta\varepsilon}{2}$ is the total strain amplitude, σ_m is the mean stress, $2N_f$ is the number of reversals to failure, σ_f' is fatigue strength coefficient ε_f' is fatigue ductility coefficient, b is fatigue strength exponent (Basquin's exponent), c is fatigue ductility exponent, and E is Young´s modulus. The strain range in the equation (3a) and (3b) is defined by the difference between the maximum and minimum strains, where the maximum strain range and the minimum strain range occur at maximum loading application and during zero loading respectively.

In contrast to stress life based mean correction factor (Gerber equation), the compressive and tensile mean stress correction factor is not the same as it is shown in Figure 2(b).

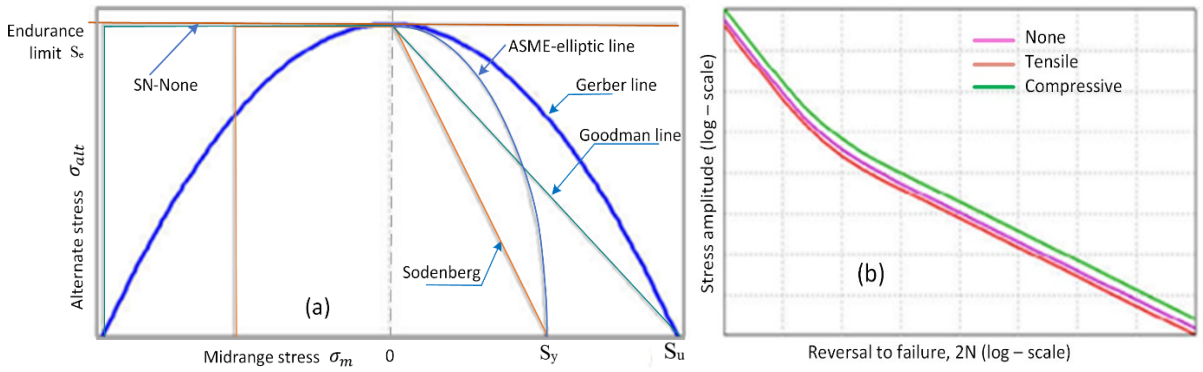

Figure 2. (a) Gerber mean stress correction factor diagram for stress life-based and (b) Morrow mean stress correction factor diagram for strain life-based method

Stress-strain response of metals is frequently altered by repeated cyclic loading. When a wheel-rail material is subjected to repeated loading cycles, accumulated plastic strain forms a cyclic closed loop curve known as hysteresis loop and the loop shows the shakedown limit at the critical location. The area within the closed loop represents the strain energy per unit volume dissipated during a cycle in the elastic-plastic regime. Mathematical expressions describing the shape of the hysteresis loop were investigated by Ramberg-Osgood equation [22] (4a) and Massing's equation (4b) [23] and these mathematical expressions are applied in the study.

$$\varepsilon = \frac{\sigma}{E} + \left(\frac{\sigma}{K'}\right)^{\frac{1}{n'}} \quad (4a)$$

$$\frac{\Delta\varepsilon}{2} = \frac{\Delta\sigma}{2E} + \left(\frac{\Delta\sigma}{2K'}\right)^{\frac{1}{n'}} \quad (4b)$$

Where $\frac{\Delta\varepsilon}{2}$ is total strain amplitude, $\frac{\Delta\sigma}{2}$ is total stress amplitude K' is cyclic strength coeficient, n' is strain hardening coefficient.

3. Result and discussion

3.1. Fatigue damage and bi-axiality indication result

Figure 3 (a) shows the maximum fatigue damage life cycle contour plot result, which is around $7x10^5$, and this damage happened in the wheel component. This demonstrates that the wheel element was subjected to high impact force and torque, allowing the fatigue damage cycle to be exploited. In accordance with wheel design assumptions, wheel elements fail earlier or give shorter service lifetime than rail track elements, demonstrating that wheel structural integrity maintenance is purposefully

designed in a softer manner than rail track for maintenance and lower initial budget expenditure. The rail track element was exposed to a minimum of 1000 fatigue damage life cycles, indicating that the rail element has a longer service life.

Unlike fatigue material property, real-world stress states are usually multiaxial. To simplify the real-world stress model, bi-axiality indication is used. The bi-axiality indication is defined as minimum principal stress divided by the maximum principal stress. A bi-axiality of 0 corresponds to uniaxial stress, bi-axiality of –1 corresponds to pure shear, and a bi-axiality of 1 corresponds to pure biaxial state or plane stress. The majority components of this model are under pure uniaxial stress, with parts exhibiting both pure shear and nearly pure bi-axiality, as shown in Figure 3(b). Considering the average stress bi-axiality, the most damaged point occurs at a point of mostly uniaxial stress and thus uniaxial stress causes fatigue damage.

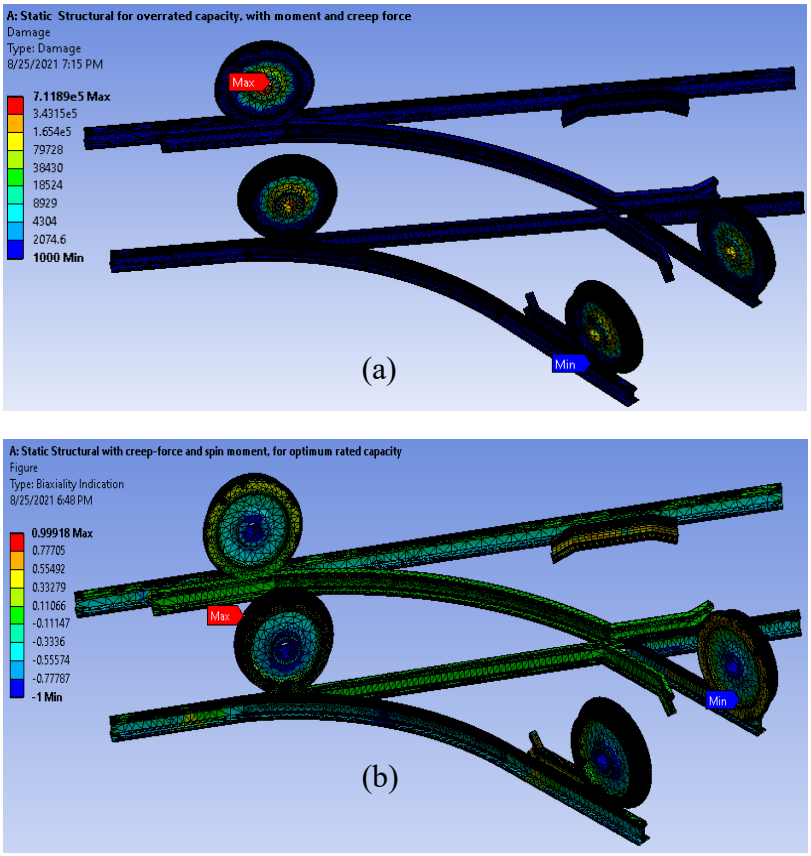

Figure 3. (a) Fatigue damage and (b) bi-axiality indication contour plot of wheel-rail contact

3.2. Fatigue sensitivity result

The fatigue sensitivity result illustrates how the fatigue characteristics change in response to varying loading at the model's critical location. For instance, if the finite element (FE) load increase by 50% or 150% of the current load, fatigue sensitivity will also change. This case requires the use of a linear fatigue sensitivity chart displayer. A value of 100% corresponds to the model's life at the actual loading case. Sensitivity may be determined in relation to life, damage, or a factor of safety. This study examines the changes of fatigue sensitivity of wheel-rail contact under three different vehicle capacity scenarios: (1) empty, (2) rated, and (3) overrated under normal and tangential contact force.

3.2.1. Empty vehicle rated capacity. The maximum and minimum fatigue sensitivity life for an empty vehicle under a normal contact force are 78900 and 1990 cycles respectively, whereas the maximum and minimum fatigue sensitivity life values under tangential contact force are 11800 and 504 cycles

respectively, Figure 4(a). Fatigue sensitivity life for normal contact force is greater than fatigue sensitivity of tangential contact force. This is because, fatigue sensitivity is dependent on the external loading. In addition, the graph plots in the figure indicate that the fatigue sensitivity is inversely proportional to the loading history.

3.2.2. Optimum vehicle rated capacity. The maximum and minimum fatigue sensitivity life under a normal contact force is 49200 and 1425 cycles and the corresponding sensitivity life values under tangential contact force are 11420 and 490 cycles respectively as shown in Figure 4(b). Therefore, fatigue sensitivity for normal contact force is greater than fatigue sensitivity of tangential contact force like in the empty vehicle case. The fatigue sensitivity life for optimum rated vehicle capacity is, however, found to be lower than that of empty vehicle capacity. This occurred due to FE load increment, as finite element load increases, fatigue resistance life decreases.

3.2.3. Overrated vehicle capacity. The maximum and minimum fatigue sensitivity life under normal contact force is 43100 and 1320 cycles and the corresponding fatigue sensitivity values under tangential contact force are 11300 and 485 cycles respectively as shown in Figure 4(c). For the overrated vehicle capacity, fatigue sensitivity for normal contact force is greater than fatigue sensitivity of tangential contact forces. For all vehicle loading cases (see Figure 4(d)), due to normal and tangential contact force increment of the FE load at rail turnouts, the life of contact surface decreases and a time to reach at fatigue resistant point or number of loading cycle is shorter.

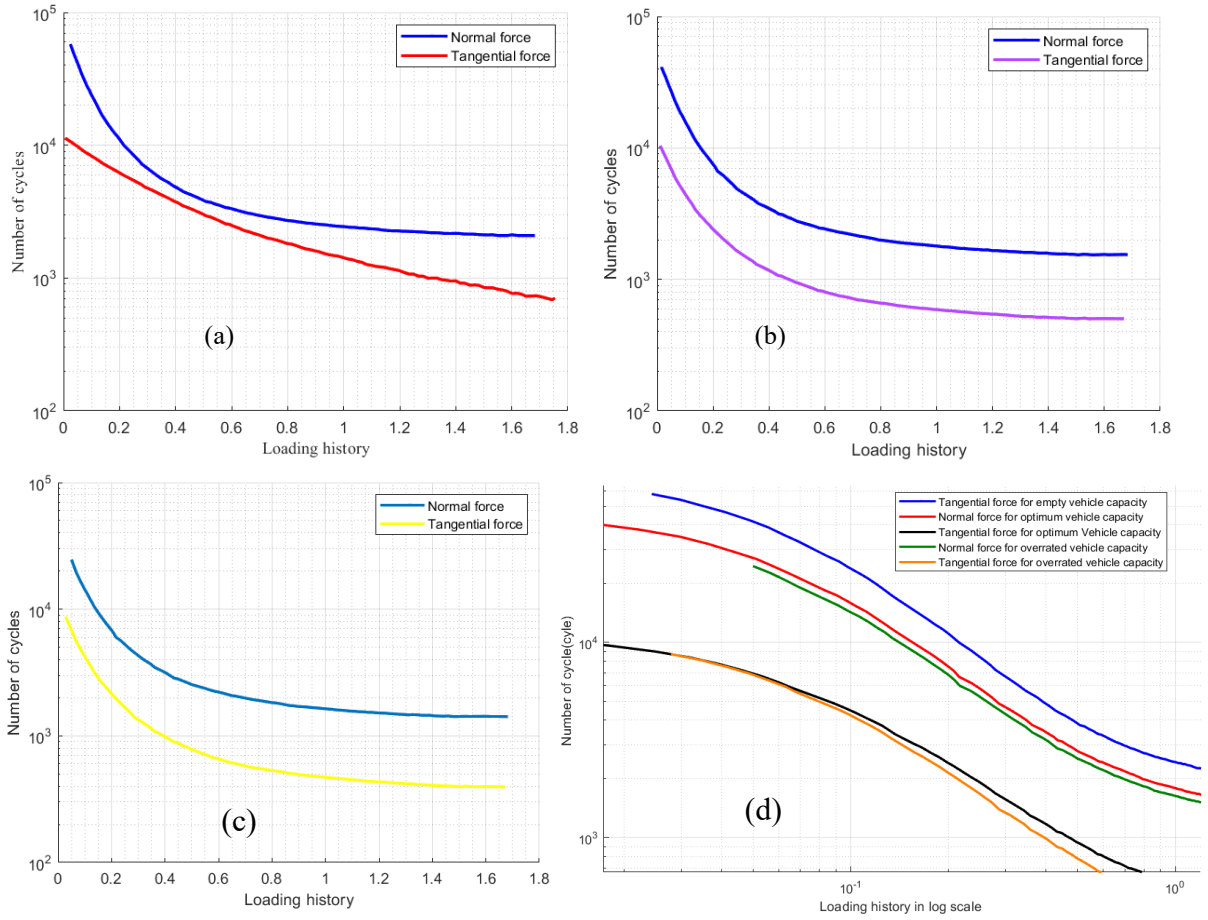

Figure 4. Fatigue sensitivity versus loading history for (a) Empty rated vehicle case, (b) Optimum rated vehicle case, (c) Overrated vehicle case (d) log-log scale for empty, optimum and overrated case

Figure 5 presents the comparison of the impact of contact forces on the fatigue sensitivity life. Clearly the normal contact force is less destructive for wheel-rail and causes fatigue damage after a higher number of loading cycles (Figure 5(a)). The tangential contact force brings about fatigue damages much earlier (Figure 5(b)).

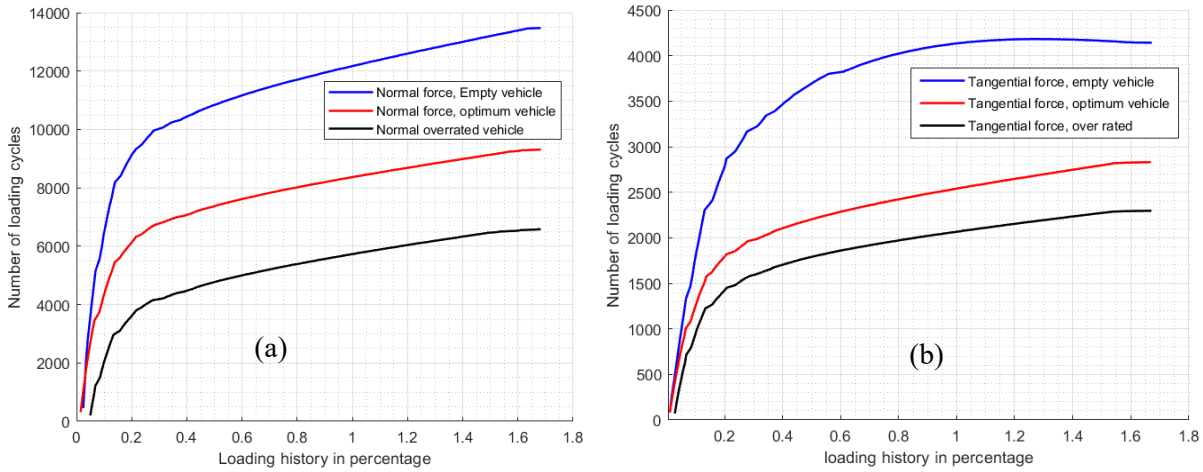

Figure 5. (a) Normal and (b) tangential contact force sensitivity

3.3. *von-Mises equivalent alternating stress result.*
The contour plot of equivalent alternating stress indicates the response of materials under repeated loading cycle for stress life-based analysis. As the loading and number of loading cycles increase, the stress formed within wheel-rail materials increases elastically up to yield strength and changes into plastic deformation if yield strength point is exceeded. This condition of equivalent alternating stress result is analysed under three different cases (empty, optimum and overrated vehicle capacity).

3.3.1. Empty vehicle capacity. The maximum equivalent alternating stress induced in the wheel-rail material is 294 MPa for a normal contact force and 500 MPa for tangential contact force as shown in the contour plot in Figure 6(a) and (b). Maximum equivalent alternating stress values under normal case is much smaller than the yield strength of wheel-rail material, i.e., 500 MPa, hence the wheel-rail material is safe in this case.

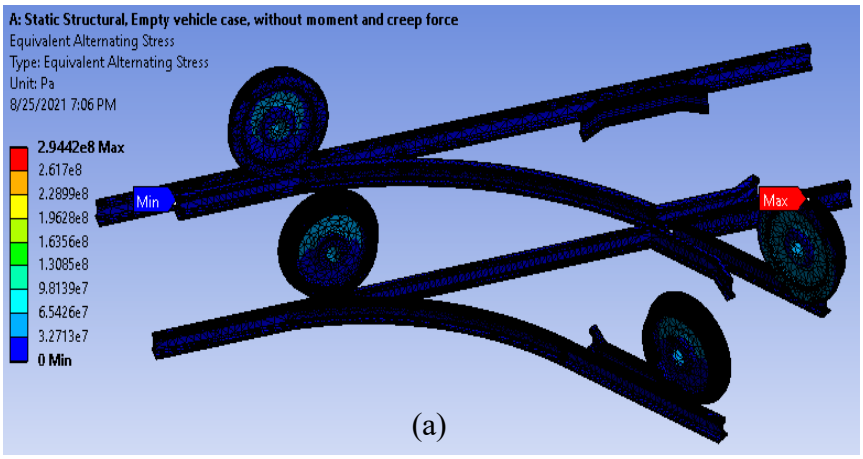

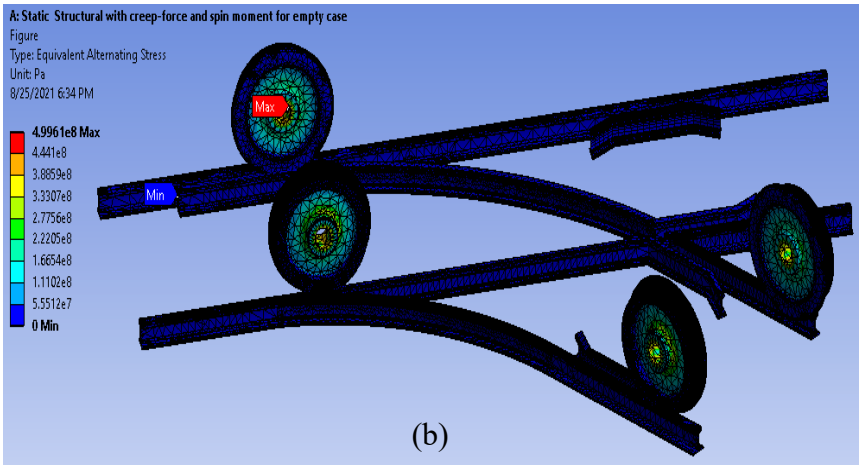

Figure 6. Von-Mises equivalent alternating stress result for empty vehicle case (a) Normal contact force case and (b) Tangential contact force case.

3.3.2. Optimum rated vehicle capacity. The maximum equivalent alternating stress formed in the wheel-rail material is 335 MPa for a normal contact force and 504 MPa for tangential contact force as shown in the contour plot in Figure 7(a) and (b). The maximum equivalent alternating stress values for normal contact force is less than the yield strength and but the maximum equivalent alternating stress values for tangential contact force exceeds the yield strength of wheel-rail materials. If these stresses repeat for several cycles, wheel-rail materials may fail under tangential contact force.

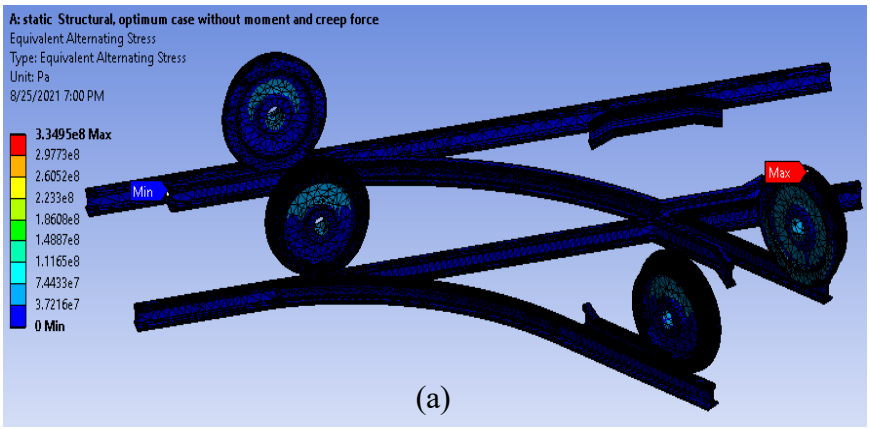

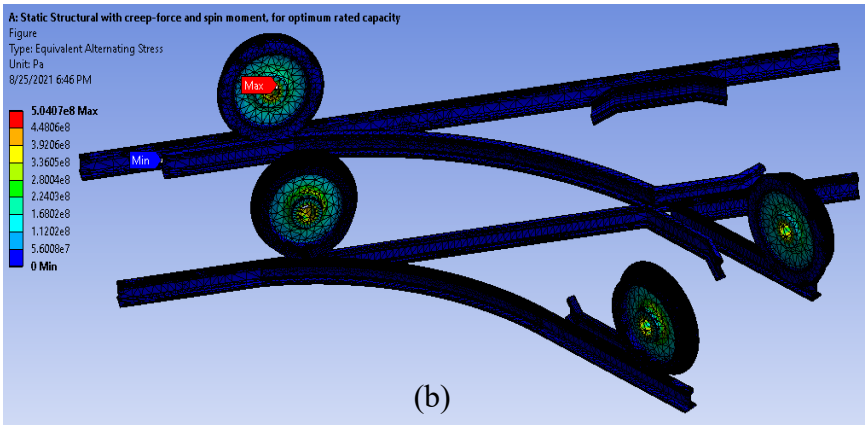

Figure 7. Von-Mises equivalent alternating stress result for optimum rated vehicle case (a) Normal contact force case and (b) Tangential contact force case.

3.3.3. Overrated vehicle capacity. For this case, the maximum equivalent alternating stress in the wheel-rail material is 345 MPa for a normal contact force and 505 MPa for tangential contact force as shown in the contour plot in Figure 8(a) and (b). The maximum and minimum equivalent alternating stresses are induced in wheel and rail material respectively. The contour plot shows that the wheel fails before the rail material which conforms with the intended design criteria of railway components. If the maximum equivalent alternating stress due to overrated vehicle capacity is repeated for several cycles, stress-induced would be greater than the yield strength of wheel-rail material, 500 MPa and wheel-rail material fails due to this alternating stress. Hence, the alternating stress under overrated vehicle capacity is dangerous.

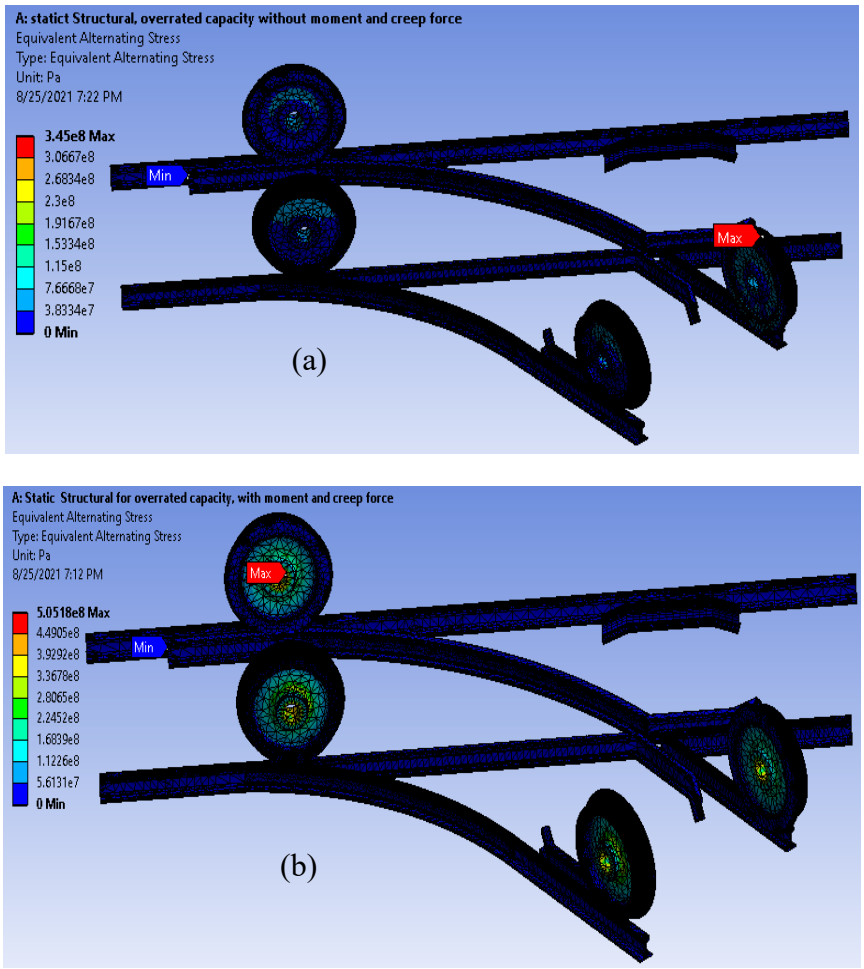

Figure 8. Von-Mises equivalent alternating stress result for overrated rated vehicle case (a) Normal contact force case and (b) Tangential contact force case.

The von-Mises equivalent alternating stress examinations give the following results, contact stress that is induced due to normal contact force for empty, optimum and overrated vehicle capacities amounts to 294 MPa, 335MPa and 345 MPa, respectively. All induced equivalent alternating stress are much lower than the yield strength, which indicates that the wheel-rail material is subjected to fatigue damage at higher number of cycles, greater than $4x10^4$cycles compared to tangential contact force. The stress values induced due to tangential contact force for empty, optimum and overrated vehicle capacities are 500 MPa, 504 MPa, and 505 MPa respectively and these stresses are nearly the same as the yield strength of wheel-rail materials, which indicates that the wheel-rail material is subjected to fatigue damage at the lower number of cycles, which is less than $1x10^4$ cycles compared to normal contact force. This indicates that if the wheel-rail materials are repeatedly subjected to tangential contact force, they will fail at lower cycles and that tangential force has a significant effect on the life of the wheel component.

3.4. Hysteresis loop/cyclic stress result

Hysteresis loop graphs are used to describe elastic-plastic behaviour of wheel-rail material with its yielding criteria. Repeated loading will form closed hysteresis loops as a result of nonlinear local stress-strain response. The Hysteresis graph plots show the strain life-based local elastic-plastic response at the critical location. The area enclosed in the hysteresis loop is the strain energy per unit volume released as heat in each loading cycle.

Hysteresis analysis is a good tool that helps to understand the true local response that may not be easy to conclude. For instance, the contour plot shown in Figure 9, indicates that although the elastic result is tensile, the local response does venture into the compressive region due to residual stresses created by the plastic response. Analysis of hysteresis loop graphs obtained using the ANSYS workbench for wheel-rail contact under three different vehicle capacities (empty, optimum and overrated) are presented and discussed as in the following subsection.

3.4.1. Empty vehicle: As shown in Figure 9(a), the maximum cyclic stress and strain amplitude values for empty vehicle capacity under normal contact force are $\pm$423 MPa and $\pm 1.56E^{-2}$ respectively. The maximum cyclic stress, $\pm$423 MPa is lower than the yield strength of wheel-rail material, 500MPa. Therefore, plastic deformation cannot start under normal contact force. As shown in Figure 9(b), the maximum cyclic stress and strain amplitude for empty vehicle capacity under tangential contact force is $\pm$511MPa and $\pm 3.72E^{-2}$ respectively.

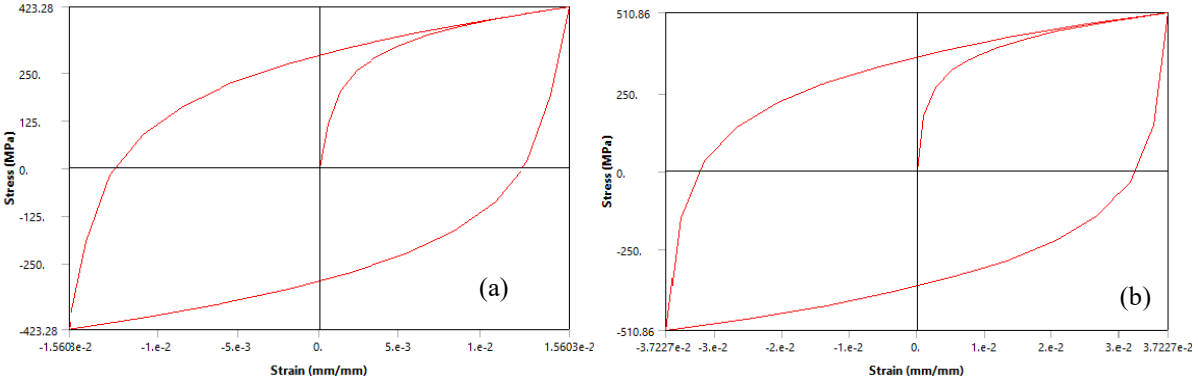

Figure 9. Hysteresis loop result for empty vehicle case (a) Normal contact force case and (b) Tangential contact force case

3.4.2. Optimum vehicle: As shown in Figure10 (a), the maximum cyclic stress and strain amplitude values under normal contact force are $\pm$444 MPa and $\pm 1.93E^{-2}$ respectively. The maximum cyclic stress, $\pm$444 MPa is lower than the yield strength of wheel-rail material, 500MPa. Therefore, plastic deformation cannot start under normal contact force for optimum rated vehicle capacity. As shown in Figure 10 (b), the maximum tensile/compressive cyclic stress and strain amplitude result for an optimum vehicle rated capacity under tangential contact force are $\pm$512 MPa and $3.78E^{-2}$ respectively. The cyclic stress is greater than yield strength of wheel-rail material which indicates that plastic deformation is initiated in wheel-rail material.

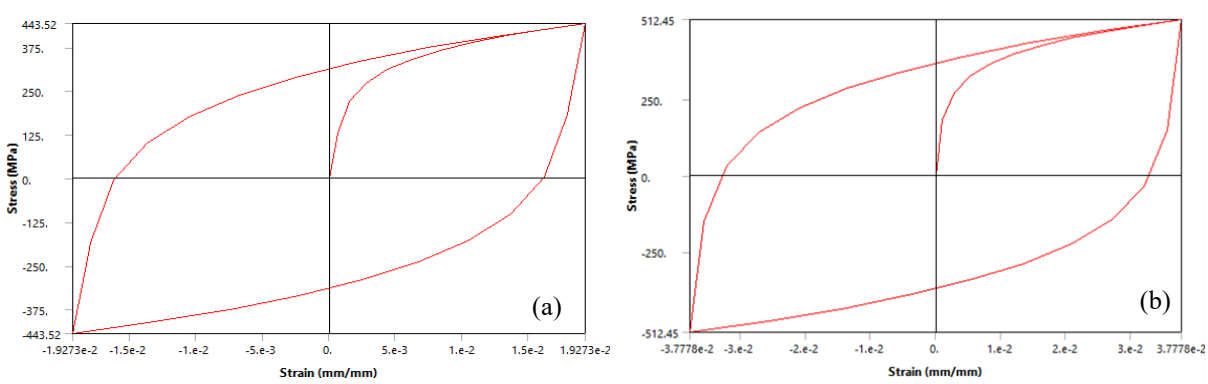

Figure 10. Hysteresis loop result for optimum rated vehicle case (a) Normal contact force case and (b) Tangential contact force case

3.4.3. Overrated vehicle: As shown in Figure 11(a), the maximum cyclic stress and strain amplitude values under normal contact force are ± 448 MPa and $\pm 2.02E^{-2}$ respectively. This indicates that the maximum tensile/compressive cyclic stress is lower than the yield strength of wheel-rail material, 500 MPa. Therefore, plastic deformation could not initiate under normal contact force for overrated vehicle capacity. As it is shown in Figure 11(b), the maximum cyclic stress and amplitude result for overrated vehicle capacity under tangential contact force are ± 513 MPa and $\pm 3.79E^{-2}$ respectively. The cyclic stress is greater than yield strength of wheel-rail material which indicates that plastic deformation is initiated in wheel-rail material.

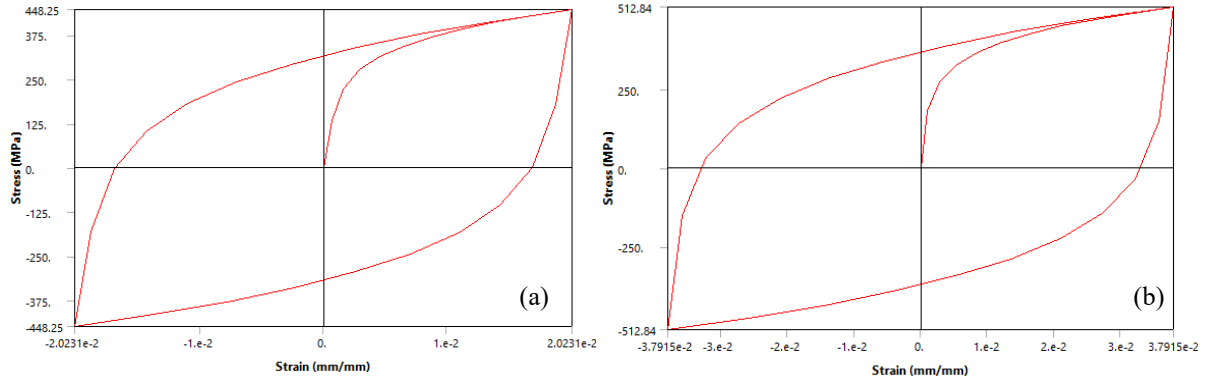

Figure 11. Hysteresis loop result for overrated vehicle case (a) Normal contact force case and (b) Tangential contact force case

The hysteresis loop results examinations give the following results, cyclic stress induced due to normal contact force for empty, optimum and overrated vehicle capacities amounts to ± 423 MPa, ± 444 MPa and ± 448 MPa, and corresponding strain are $\pm 1.56E^{-2}$, $\pm 1.93E^{-2}$ and $\pm 2.02E^{-2}$ respectively. All induced cyclic stress is much lower than the yield strength, which indicates that the wheel-rail material is subjected to excessive deformation at higher number of cycles, compared to tangential contact force. The cyclic stress values induced due to tangential contact force for empty, optimum and overrated vehicle capacities are ± 500 MPa, ± 512 MPa and ± 513 MPa, and corresponding strain are $\pm 3.72E^{-2}$, $\pm 3.78E^{-2}$ and $\pm 3.79E^{-2}$ respectively and these stresses are greater than the yield strength of wheel-rail materials, which indicates that the wheel-rail material is subjected to fatigue damage and excessive deformation at the lower number of cycles, compared to normal contact force.

4. Conclusion

A part of the work done on fatigue life analysis of wheel-rail contact at railway turnouts using finite element modelling approach is presented in this article. Tools available in the static structural analysis toolbox of the ANSYS workbench supported the examination of the fatigue life, fatigue sensitivity, alternating stress, and cyclic stress of wheel-rail contact based on the operational parameters of an Ethiopian railway company (Addis Ababa Light Rail Transit). The effects of turnout geometry, normal and tangential contact force has on a fatigue sensitivity life, alternating contact stress, and hysteresis loop stresses are investigated and presented. For different vehicle loading conditions (empty, optimum, and overrated), the maximum fatigue sensitivity life obtained under normal force is 78900, 49200, and 43100 cycles, whereas it is 11800, 11420, and 11300 cycles under tangential force, respectively. This leads to the conclusion that normal contact force can withstand additional loading cycles up to seven times greater than tangential contact force, implying that tangential contact force reduces the life of contacting surfaces. In contrast to fatigue sensitivity, the maximum von-Mises equivalent alternating and hysteresis loop stresses caused by tangential contact force are substantially higher than normal contact force. These stresses cause rolling contact fatigue and excessive deformation, which shortens the contacting surface's life cycle. In comparison to the normal contact force, the tangential contact force has a considerable influence on the fatigue sensitivity life cycle, and wheel-rail material is exposed to fatigue degradation at lower cycles. According to the finite element modelling of the study done, contact force types and track geometry have a significant impact on contact damages and structural integrity.

References

[1]. Skrypnyk R, Ossberger U, Pålsson BA, Ekh M and Nielsen J C O 2021 Long-term rail profile damage in a railway crossing: Field measurements and numerical simulations. *Wear*, **472–473**, 1–13. https://doi.org/10.1016/j.wear.2020.203331.

[2]. Xu J, Gao Y, Wang P, An B, Chen J and Chen R 2020 Numerical analysis for investigating wheel-rail impact contact in a flange bearing frog crossing. *Wear*, **450–451**, 203253. https://doi.org/10.1016/j.wear.2020.203253.

[3]. Wei Z, Núñez A, Liu X, Dollevoet R and Li Z 2020 Multi-criteria evaluation of wheel/rail degradation at railway crossings. *Tribol Int.***144**. https://doi.org/10.1016/j.triboint.2019.106107.

[4]. Lu C, Rodríguez-Arana B, Prada J G., Meléndez J and Martínez-Esnaola J M 2020 A full explicit finite element simulation for the study of interaction between wheelset and switch panel. *Vehicle System Dynamics.* **58**(2), 229–248. https://doi.org/10.1080/00423114.2019.1575425.

[5]. Sysyn M, Kluge F, Gruen D, Kovalchuk V and Nabochenko O 2019 Experimental analysis of rail contact fatigue damage on frog rail of fixed common crossing 1:12. *J Fail Prev.* **19**(4), 1077–1092. https://doi.org/10.1007/s11668-019-00696-w.

[6]. Chen R, Chen J, Wang P, Fang J and Xu J 2019 Impact of wheel profile evolution on wheel-rail dynamic interaction and surface initiated rolling contact fatigue in turnouts. *Wear*, **438–439**, 203109. https://doi.org/10.1016/j.wear.2019.203109.

[7]. Skrypnyk R, Nielsen, J C O, Ekh M and Pålsson B A 2019 Metamodelling of wheel–rail normal contact in railway crossings with elasto-plastic material behaviour. *Eng Comput*, **35**(1), 139–155. https://doi.org/10.1007/s00366-018-0589-3.

[8]. Skrypnyk R, Ekh M, Nielsen, J C O and Pålsson B A 2019 Prediction of plastic deformation and wear in railway crossings – Comparing the performance of two rail steel grades. *Wear*, **428–429**, 302–314. https://doi.org/10.1016/j.wear.2019.03.019.

[9]. Xu L and Liu X 2021 Matrix coupled model for the vehicle–track interaction analysis featured to the railway crossing. *Mech Syst Sig Process.***152**, 107485. https://doi.org/10.1016/j.ymssp.2020.107485.

[10]. Grossoni I, Hughes P, Bezin Y, Bevan A and Jaiswal J 2021 Observed failures at railway turnouts: Failure analysis, possible causes and links to current and future research. *Eng Fail Anal*. **119**, 104987. https://doi.org/10.1016/j.engfailanal.2020.104987.

[11]. Katheriya P, Kumar V, Choudhary A and Raji, N 2014 An investigation of effects of axle load and train speed at rail joint using finite element method. *Int J Res Eng Technol.* **3**(08), 41–47.

[12]. Özdemir, Y., & Voltr, P. 2016. Analysis of the wheel and rail frictionless normal contact considering material parameters. *J Appl Math Compu Mech.***15**(2), 95–103.

[13]. Jelila Y D and Lemu, H G 2021 Study of wheel-rail contacts at railway turnout using multibody dynamics simulation approach. *Int. Workshop Adv Manuf Autom.* **2**, 371–379. https://doi.org/10.1007/978-981-33-6318-2_46.
[14]. Zaazaa K E and Schwab A L 2009 Review of joost Kalker's wheel-rail contact theories and their implementation in multibody codes. *Proc ASME Des Eng Techn Conf*. **4**(PARTS A, B AND C), 1889–1900. https://doi.org/10.1115/DETC2009-87655.
[15]. Browell R and Hancq A 2006 *Calculating and Displaying Fatigue Results, ANSYS Technical Notes,* (Issue 29), available at http://aes.nu/publications/2006-technotes-ANSYS_Fatigue.pdf.
[16]. Gerber, T. L, and Fuchs, H O 1970 Improvement in the fatigue strength of notched bars by compressive self-stresses, In: *Achievement of High Fatigue Resistance in Metals and Alloys*, ASTM International, 276-95.
[17]. Liu Y and Mahadevan S 2005 Multiaxial high-cycle fatigue criterion and life prediction for metals. *Int J Fatigue.***27**(7), 790–800. https://doi.org/10.1016/j.ijfatigue.2005.01.003.
[18]. Zhang J L, Shang DG, Sun Y J and Wang X W 2018 Multiaxial high-cycle fatigue life prediction model based on the critical plane approach considering mean stress effects. *Int J Damage Mech.* **27**(1), 32–46. https://doi.org/10.1177/1056789516659331.
[19]. Manson, S S, and Halford, G R 1981 Practical implementation of the double linear damage rule and damage curve approach for treating cumulative fatigue damage, *Int J fract*, 17(2), 169-192.
[20]. Morrow J 1968 Fatigue properties in metal, Fatigue Design Handbook, Advances in Engineering, Vol. 4 Society of Automotive Engineers, Warrendale, PA, USA, pp. 21-29.
[21]. Pun C L, Kan Q, Mutton P J, Kang G and Yan W 2014 A single parameter to evaluate stress state in rail head for rolling contact fatigue analysis. *Fatigue Fract Eng Mater Struct.* **37**(8), 909–919. https://doi.org/10.1111/ffe.12157.
[22]. Ramberg W and Osgood, W. R. 1943 Description of stress–strain curves by three parameters. *Technical Note No. 902*, National Advisory Committee for Aeronautics, Washington DC.
[23]. Vyas N S, Sidharth and Rao J S 1997 Dynamic stress analysis and a fracture mechanics approach to life prediction of turbine blades, *Mech Mach Theory* **32**, 511 – 527.